Biomaterials and Biosystems 5 (2022) 100032

Contents lists available at ScienceDirect

Biomaterials and Biosystems

journal homepage: www.elsevier.com/locate/bbiosy

# Spacer length and serum protein adsorption affect active targeting of trastuzumab-modified nanoparticles

Christina Barth[a], Hendrik Spreen[a], Dennis Mulac[a], Lucas Keuter[b], Matthias Behrens[b], Hans-Ulrich Humpf[b], Klaus Langer[a,*]

[a] Institute of Pharmaceutical Technology and Biopharmacy, University of Muenster, Corrensstr. 48, 48149 Muenster, Germany
[b] Institute of Food Chemistry, University of Muenster, Corrensstr. 45, 48149 Muenster, Germany

ARTICLE INFO

*Keywords:*
Nanoparticles
Human serum albumin
Polyethylene glycol
Trastuzumab
Active targeting
Protein corona
Human serum
Proteomics

ABSTRACT

Receptor-mediated active targeting of nanocarriers is a widely investigated approach to specifically address cancerous cells and tissues in the human body. The idea is to use these formulations as drug carriers with enhanced specificity and therefore reduced systemic side effects. Until today a big obstacle to reach this goal remains the adsorption of serum proteins to the nanocarrier's surface after contact with biological fluids. In this context different nanoparticle characteristics could be beneficial for effective active targeting after formation of a protein corona which need to be identified. In this study trastuzumab was used as an active targeting ligand which was covalently attached to human serum albumin nanoparticles. For coupling reaction different molecular weight spacers were used and resulting physicochemical nanoparticle characteristics were evaluated. The *in vitro* cell association of the different nanoparticle formulations was tested in cell culture experiments with or without fetal bovine serum. For specific receptor-mediated cell interaction SK-BR-3 breast cancer cells with human epidermal growth factor receptor 2 (HER2) overexpression were used. MCF-7 breast cancer cells with normal HER2 expression served as control. Furthermore, serum protein adsorption on respective nanoparticles was characterized. The qualitative and quantitative composition of the protein corona was analyzed by SDS-PAGE and LC-MS/MS and the influence of protein adsorption on active targeting capability was determined.

## 1. Introduction

Looking at modern cancer therapy, a great variety of approved pharmaceuticals is available. The first group of drugs used for this purpose were cytostatic drugs with low tumor specificity and high toxicity. As of today, the portfolio of available pharmaceuticals has increased over the last 20 years and new "modern" therapeutics like monoclonal antibodies, small molecule inhibitors and recently chimeric antigen receptor T-cells have been approved [1]. In contrast to conventional chemotherapeutics, antibodies and small molecule inhibitors were developed to address specific structures mainly expressed on cancer cells. Structures include overexpressed receptors like human epidermal growth factor receptor 2 (HER2), transferrin receptor and folate receptor [2,3].

A promising idea on which intensive research was focused on in the last years is combining nanoparticulate drug carriers with targeting ligands. For this purpose, ligands either address structures overexpressed on tumor cells or structures only present on tumor cells [4]. This so-called active targeting has the following advantages: reduction of the systemic side effects of cytostatic drugs and improved drug delivery efficiency. Possible active targeting ligands for such systems can be peptides, proteins, antibodies or fragments of them [5].

In this study the monoclonal antibody trastuzumab was used as active targeting ligand addressing HER2. Trastuzumab is an approved drug for HER2 overexpressing early and metastatic breast cancer, as well as HER2 overexpressing metastatic gastric cancer [6]. Furthermore, the antibody is already well established as active targeting ligand for various nanoparticle (NP) formulations [7–9]. As a commonly used NP matrix human serum albumin (HSA) was utilized. HSA has already been tested as a drug delivery system for cytostatic drugs like doxorubicin and paclitaxel [10,11]. Additionally, the NP surface was grafted with different molecular weight polyethylene glycol (PEG) derivatives. PEG represents an ideal crosslinker for covalent attachment of targeting ligands because of the availability of many different end groups [12]. PEG also mediates stealth effects *in vivo* reducing serum protein adsorption and consequently resulting in a prolonged blood circulation time. These effects are dependent on the density and the molecular weight of the linear PEG [13].

Serum protein adsorption with formation of a protein corona occurs whenever NPs get into contact with biological fluids like blood, result-

* To whom correspondence should be addressed.
*E-mail address:* k.langer@uni-muenster.de (K. Langer).

https://doi.org/10.1016/j.bbiosy.2021.100032
Received 14 July 2021; Received in revised form 15 November 2021; Accepted 9 December 2021

ing in a new NP biological identity [5,14,15]. Hence, blood circulation time, biodistribution and targeting of nanocarriers can be influenced. The NP characteristics like size, shape and surface composition, as well as environmental parameters like temperature and type of fluid can affect the composition of the protein corona [16,17]. Corona proteins can either act as opsonins and mark NPs for rapid recognition by the reticuloendothelial system or they act as dysopsonins mediating longer blood circulation times [18]. As PEG can reduce protein adsorption, but not completely prevent it, the formation of a protein corona around the NPs has to be considered for successful active targeting.

The aim of this study was on the one hand to analyze the effect of different PEG spacers with varying length for ligand coupling on active targeting. On the other hand, we aimed to characterize the protein corona formed around these NPs and its influence on the active targeting capability. We demonstrated that both serum protein adsorption and selection of the PEG spacer for the targeting moiety have an effect on active targeting and also influence each other.

## 2. Materials and methods

### 2.1. Materials

Human serum albumin (purity ≥ 96%), glutaraldehyde 50% (m/v) solution, 2-iminothiolane, and IgG from rabbit serum were purchased from Sigma Aldrich (Steinheim, Germany). *N*-Hydroxysuccinimide-PEG-maleimide spacers were obtained from Rapp Polymere (Tübingen, Germany) and m-maleimidobenzoyl-*N*-hydroxysulfosuccinimide ester (sMBS) was obtained from CovaChem LLC (Loves Park, IL, USA). Trastuzumab was purchased as Herceptin® from Roche (Welwyn Garden City, UK) and the fluorescent dye PromoFluor-505 NHS-ester was purchased from PromoCell GmbH (Heidelberg, Germany). For serum protein adsorption pooled human serum (HS) of the same lot from Biowest (Riverside, MO, USA) was used. All reagents for sodium dodecyl sulfate-polyacrylamide gel electrophoresis (SDS-PAGE) (Roti®-Load 1, ammonium peroxodisulfate (APS), SDS, tetramethylethylenediamine (TEMED), Rotiphorese® Gel 30, Rotiphorese® 10 x SDS-PAGE, Roti®-Mark STANDARD, Roti®-Blue) were obtained from Carl Roth GmbH & Co. KG (Karlsruhe, Germany). For LC-MS/MS analysis urea was purchased from Acros Organics (Fair Lawn, NJ, USA). DL-dithiothreitol (DTT) and iodoacetamide (IAA) were purchased from Sigma Aldrich (Steinheim, Germany). Trypsin (sequencing grade) was obtained from Promega Corp. (Madison, WI, USA), acetonitrile was obtained from Fisher Scientific (Hampton, NH, USA), isopropanol (LC-MS grade) was purchased from Carl Roth GmbH & Co. KG (Karlsruhe, Germany), sodium hydroxide was obtained from Grüssing (Filsum, Germany) and formic acid (98–100%) was obtained from Merck KGaA (Darmstadt, Germany).

MCF-7 cells were kindly provided by Dr. Spänkuch (Universitäts-Frauenklinik, Tübingen) and SK-BR-3 cells were purchased from ATCC® (LGC Standards GmbH, Wesel, Germany). Cell culture media (McCoy's 5A modified Medium and Dulbecco's Modified Eagle Medium (DMEM)), trypsin/EDTA solution, as well as the supplements, glutamine, non-essential amino acids (NEA), penicillin/streptomycin, gentamicin, fetal bovine serum (FBS), and phosphate-buffered saline (PBS) were obtained from Biochrom AG (Berlin, Germany). Human epidermal growth factor (EGF) was purchased from Roche Diagnostics (Mannheim, Germany) and paraformaldehyde was purchased from Sigma Aldrich (Steinheim, Germany).

### 2.2. Preparation of antibody-modified nanoparticles

Antibody-modified NPs were prepared based on a previously described method [7]. In brief, HSA was dissolved in 1.0 mL of purified water to a concentration of 50 mg/mL and the pH was adjusted to 7.0. A total of 4 mL of ethanol (96%, v/v) were added to the HSA solution dropwise resulting in desolvation and NP formation. The NPs were stabilized by adding 29.5 µL glutaraldehyde (8%, m/v) and overnight stirring (550 rpm, 22 °C). Afterwards the NPs were purified by two steps of centrifugation (10,500 × *g*, 14 min) and redispersion in 1.0 mL phosphate buffer (pH 8.0).

Subsequently the NP surface was modified with a heterobifunctional crosslinker. *N*-Hydroxysuccinimide-PEG-maleimide spacers with a molecular weight of 3 kDa ($PEG_3$), 5 kDa ($PEG_5$), and 10 kDa ($PEG_{10}$) as well as sMBS were used. A 15-fold molar excess of crosslinker relative to HSA was dissolved in DMSO and added to the NP suspension containing 25 mg of NPs. The mixture was stirred for 1 h at 600 rpm and 22 °C, followed by one step of centrifugation (12,000 × *g*, 14 min) and redispersion in 1.0 mL phosphate buffer (pH 8.0). The supernatants were collected and analyzed via size exclusion chromatography (SEC) for unreacted PEG crosslinker (Fig. S1).

Parallel to this reaction an aliquot of 0.5 mL trastuzumab (5 mg/mL in phosphate buffer pH 8.0) was purified by SEC with a PD-10 Sephadex™ G-25 M desalting column (GE Healthcare Europe GmbH, Freiburg, Germany) using phosphate buffer pH 8.0 as eluent. The fractions containing antibody were determined using UV/Vis spectroscopy at 280 nm and combined afterwards. For the introduction of thiol groups on the antibody surface, 1.0 mL of purified trastuzumab or 1.0 mL IgG (1 mg/mL) were incubated with 40.2 µL 2-iminothiolane (1.14 mg/mL, 50-fold molar excess) for 2 h at 600 rpm and 22 °C. Afterwards, the thiolated antibody was purified by SEC as described above, resulting in an antibody concentration of about 0.5 mg/mL.

For covalent coupling of the antibody to the surface-modified NPs an aliquot of 1.0 mL of the thiolated antibody (500 µg) was incubated with the NP suspension (equivalent to 20 mg NPs) over night at 600 rpm and 22 °C. Antibody-modified NPs were purified by centrifugation (7000 × *g*, 14 min) and redispersion in purified water. The supernatant was collected and the unreacted thiolated antibody was determined by SEC (Fig. S2).

For cell culture experiments HSA was labeled with a fluorescent dye prior to NP preparation. A previously described method by Keuth et al. [19] was used for labeling HSA with a PromoFluor-505-NHS-ester (PF).

### 2.3. Nanoparticle characterization

Hydrodynamic particle diameter and polydispersity index (PDI) were determined by photon correlation spectroscopy. An aqueous dilution of the NP suspension was analyzed at 22 °C and a backscattering angle of 173°. For surface charge characterization the zeta potential was determined using the same aqueous dilution of the NP suspension. All measurements were conducted with a Malvern Zetasizer Nano ZS system (Malvern Instruments Ltd., Malvern, UK).

NP concentration was determined gravimetrically by drying 20.0 µL of NP suspension to mass consistency for at least 2 h at 80 °C.

### 2.4. Adsorption of serum proteins on nanoparticles

As described before, NP suspensions were adjusted to a constant surface-to-protein ratio [20,21]. The required amount of NP suspension for a predefined particle surface was calculated based on hydrodynamic diameter, particle density (1.31 g/cm$^3$ [22]), and particle concentration. For SDS-PAGE analysis, an aliquot equivalent to 0.08 m$^2$ NP surface was diluted to 1.730 mL with purified water. The protein corona was formed by adding 270 µL of HS (70.8 mg/mL) and incubation for 30 min at 37 °C under constant shaking (1200 rpm). Samples were purified from excess proteins by three steps of centrifugation (20,000 × *g*, 20 min) and redispersion in purified water.

For LC-MS/MS analysis a higher amount of protein was used. Therefore, NP surface was tripled to 0.24 m$^2$ and NP suspensions were diluted to 5.190 mL with purified water. To maintain a constant NP surface-to-protein ratio, the amount of HS was also tripled to 810 µL. Incubation and purification followed as described above.

### 2.5. SDS-PAGE analysis of bound corona proteins

After the previously described adsorption of serum proteins and the subsequent purification, the NP pellet was resuspended in 30 μL SDS-containing loading buffer (Roti®-Load 1) overnight (1200 rpm, 22 °C) to desorb the proteins from the NP surface. The desorbed proteins were separated from the NPs by centrifugation (30,000 × *g*, 45 min) and the corona proteins remaining in the supernatant were denatured for 5 min at 95 °C.

A 10% polyacrylamide gel was prepared by mixing 1.975 mL water, 1.675 mL acrylamide solution (30%, m/v, Rotiphorese® Gel 30), 1.25 mL separation gel buffer, 50 μL SDS solution (10%, m/v), 50 μL APS solution (10%, m/v), and 5 μL TEMED and transferring the solution to an OmniPAGE mini system gel chamber (Omnilab-Laborzentrum GmbH & Co. KG, Bremen, Germany). A focusing gel was positioned on top of the separation gel by mixing 2.1 mL water, 500 μL acrylamide solution (30%, m/v), 380 μL focusing gel buffer, 30 μL SDS solution (10%, m/v), 30 μL APS solution (10%, m/v), and 3 μL TEMED. Samples (8 μL), positive controls (8 μL) and a protein standard (5 μL, Roti®-Mark STANDARD) were applied onto the gel and separated under a constant voltage of 200 V for 90 min. Following separation, the protein bands were fixed with 1% orthophosphoric acid in methanol/water (1 + 4, v/v), stained with Coomassie Brilliant Blue G-250 and excess staining was eliminated by washing with methanol/water (1 + 2, v/v). The resulting gel was visualized using a Gel iX Imager (INTAS Science Imaging Instruments GmbH, Göttingen, Germany).

### 2.6. LC-MS/MS analysis of bound corona proteins

#### 2.6.1. Sample preparation

Serum proteins were adsorbed onto the NP surface and purification from excess proteins followed as described above. The following sample preparation steps for a bottom-up LC-MS/MS approach were performed based on protocols by Partikel et al. [17] and Wisniewski et al. [23]. After the last step of centrifugation, the purified NP pellet was incubated with 100 μL of 6 M urea in TRIS buffer (pH 7.8) overnight (1200 rpm, 22 °C) to desorb the serum proteins from the NP surface. The desorbed proteins were separated from the NP pellet by collecting the supernatant after centrifugation (30,000 × *g*, 45 min). The total amount of protein per sample was quantified using a Pierce™ BCA Protein Assay Kit (Thermo Fisher Scientific Inc., Rockford, IL, USA). For reduction of disulfide bonds, samples were incubated with 5 μL 200 mM DTT for 1 h (1200 rpm). Afterwards, aliquots containing a maximum of 250 μg of protein were transferred to Microcon® 30 kDa filter units and centrifuged (14,000 × *g*, 15 min). The flow-through was discarded after the addition of 200 μL 8 M urea in TRIS buffer (pH 8.5) to the filter units and another step of centrifugation (14,000 × *g*, 15 min). Subsequently, 100 μL 50 mM IAA in 8 M urea solution were added to the filter units, mixed for 1 min (600 rpm) and incubated for another 20 min without shaking. The proteins on the filter units were washed three times by adding 100 μL 8 M urea solution, centrifugation (14,000 × *g*, 15 min) and discarding the flow-through afterwards. Three steps of adding 100 μL 50 mM ammonium bicarbonate ($NH_4HCO_3$) solution to the filter units, centrifugation (14,000 × *g*, 10 min) and discarding the flow-through followed. For tryptic digestion, 20 μL of cooled trypsin solution (0.2 μg/mL) and 40 μL of cooled $NH_4HCO_3$ solution were added to the filter units and incubated for 1 min under constant shaking (600 rpm). Thereafter, filter units were incubated at 37 °C, 100% humidity and gentle shaking overnight. After digestion, the filter units were transferred to new collection tubes and centrifuged (14,000 × *g*, 10 min), followed by adding 40 μL $NH_4HCO_3$ solution and another step of centrifugation (14,000 × *g*, 10 min). The flow-through of the last two steps of centrifugation, containing the digested peptides, was collected. Aliquots of the same sample were merged, acidified to a pH < 4 with formic acid and diluted to 2.0 mL with purified water.

Solid-phase extraction was used to desalt the samples prior to LC-MS/MS analysis. Strata™-X 33u RP 30 mg/1 mL columns (Phenomenex, Aschaffenburg, Germany) were activated with 1 mL methanol, equilibrated with 1 mL aqueous formic acid (1%, v/v) and the peptide solution was applied in fractions of 1.0 mL. The samples were washed with 1.0 mL of purified water and eluted with 600 μL 1% formic acid in methanol/water (1 + 1, v/v) and 400 μL 1% formic acid in methanol/water (7 + 3, v/v). The eluted peptides were concentrated by evaporation of the solvent under nitrogen atmosphere and dissolved in 100 μL 1% formic acid in acetonitrile/water (3 + 97, v/v). Samples were stored at −20 °C until analysis.

#### 2.6.2. Data acquisition

Prepared samples with peptides were separated with a Bruker Elute HAT HPG 1300 LC system equipped with a Bruker PAL Autosampler, a Bruker Column Oven (all Bruker Daltonics, Bremen, Germany) and an Agilent AdvanceBio Peptide Mapping column (120 Å, 2.1 × 150 mm, 2.7 μm, Agilent Technologies, Santa Clara, CA, USA). For data-dependent acquisition (DDA) and data-independent acquisition (DIA) measurements, an aliquot of 10.0 μL was injected and eluted at a flow rate of 0.2 mL/min at a temperature of 40 °C. A gradient of acetonitrile and water (both supplemented with 0.1% formic acid, Table S1) with a total run time of 110 min for DDA and 22 min for DIA was used. KrudKatcher Classic HPLC in-line filters (0.5 μm, Phenomenex, Aschaffenburg, Deutschland) were employed to protect the column. Data acquisition was performed with Bruker HyStar v4.1 SR 2 (4.1.31.1) software. For mass calibration 10 mM sodium formate in isopropanol/water (1 + 1, v/v) was applied at a flow rate of 3 μL/min in the first minute of each run.

A Bruker Impact II quadrupole time-of-flight mass spectrometer was utilized with Bruker Compass software 2.0 v4.1 (Build 3.9, both Bruker Daltonics, Bremen, Germany). For profile data acquisition, instrument settings were set as follows: ESI in positive mode with an endplate offset of 500 V; capillary voltage of 4500 V, $N_2$ as nebulizer gas at 4 bars with a dry gas flow of 12 L/min and a dry gas temperature of 250 °C; scan rate of 2 Hz and a mass range of *m/z* 150–2200. Collision RF was set as 2000 Vpp with 90 μs of transfer time and 10 μs pre-pulse storage time.

For DDA measurements, collision energy was set to 23–65 eV depending on the mass-to-charge ratio and charge state of the peptide precursor. Precursor ions with a mass-to-charge ratio of 2–5, a charge > 1 and a mass range of *m/z* 300–2200 were considered for fragmentation in Auto MS/MS mode. The scan rate for fragment ions was 8 Hz (≥ 2500 counts) or 32 Hz (> 25,000 counts) with a cycle time of 3 s.

For DIA measurements, a sequential window acquisition of all theoretical fragment ion mass spectra (SWATH) approach was used. Sequential precursor windows in a mass range of *m/z* 400-1200 were fragmented and analyzed. To increase the selectivity, window width was adjusted according to the abundance of different peptides in the respective *m/z* range (Table S2). Precursor windows were overlapping and windows were chosen to approximately contain the same number of peptides [24]. Collision energy was set to 27–48 eV depending on mass-to-charge ratio and scan rate for fragment ions was set to 16 Hz. Including the total ion scan (*m/z* 150–2200) resulted in a total scan time of 0.9375 s.

Data processing was accomplished automatically with Bruker Data Analysis v4.4 (Build 200.55.2969) using the *Shotgun Digest Protein Analysis method* for DDA acquisition method and sodium formate calibration for die DIA acquisition method.

#### 2.6.3. Data analysis

*2.6.3.1. Qualitative analysis.* For protein identification a *de novo*-assisted database search algorithm was used (PEAKS® Studio 7, Bioinformatics Solutions Inc., Waterloo, Canada) against the UniProt KB database (*Homo sapiens*, created 2020–11–02). In addition, the enhanced target-decoy method (*decoy fusion*) was used for result validation and false discovery rate estimation. Search parameters were set

with trypsin as specific enzyme (three missed cleavages allowed), carbamidomethylation of cysteine residues (fixed) and oxidation of methionine (variable, three PTM per peptide allowed). A precursor mass tolerance of 5 ppm and a fragment mass error tolerance of 1 Da was accepted. Only proteins with a -lgP value > 80 and a minimum of 1 unique peptide sequence were considered as reliable [25].

*2.6.3.2. Quantitative analysis.* For protein quantitation of SWATH measurements, Skyline 20.2 software (MacCoss Lab Software, University of Washington, Seattle, WA, USA) was used. Peptide and transition settings were set as shown in Table S3. Representative peptides for protein quantitation were selected based on dotp/idotp value (> 0.8), retention time matching the predicted retention time and mass error (< 10 ppm). For evaluated proteins, the peak area of one peptide precursor matching the before defined quality criteria was analyzed. Detailed information on the used precursors is listed in Table S4.

### 2.7. Cell culture studies

#### 2.7.1. Cell lines and cultivation

For cell culture studies two different breast cancer cell lines were used, namely MCF-7 cells with regular HER2 expression and SK-BR-3 cells with HER2 overexpression. MCF-7 cells were cultivated in 75 $cm^2$ flasks using DMEM supplemented with 1% (v/v) glutamine (200 mM), 1% (v/v) NEA, 100 U/mL penicillin, 100 µg/mL streptomycin, and 10% (v/v) FBS. SK-BR-3 cells were cultivated in cell culture dishes (Ø 60 mm) using McCoy's 5A modified Medium supplemented with 1% (v/v) glutamine (200 mM), 100 µg/mL gentamicin, 500 µL EGF (10 µg/mL), and 20% (v/v) FBS. Both cell lines were cultivated in an incubator at 100% humidity, 37 °C and 10% $CO_2$ for MCF-7 cells and 5% $CO_2$ for SK-BR-3 cells. After reaching about 80% confluency, cells were split at a ratio of 1:1 to 1:3 twice a week. All experiments were carried out within the first 20 passages after thawing.

For serum free conditions DMEM supplemented with 1% (v/v) glutamine (200 mM), 1% (v/v) NEA, 100 U/mL penicillin, 100 µg/mL streptomycin, and 1% (v/v) gentamicin (10 mg/mL) was used.

#### 2.7.2. Determination of cellular interaction by flow cytometry

To evaluate the interaction of antibody-modified NPs with the different HER2 expressing breast cancer cell lines, flow cytometric analysis was conducted. Cells were seeded on 24 well plates with $1 \times 10^5$ cells/well and cultivated for 48 h. NPs were diluted in respective cell culture medium and two wells were incubated with each NP formulation in a concentration of 50 µg/mL for 0.5, 1, 2, 4, and 24 h. After incubation, cells were washed with PBS and harvested by detaching with trypsin/EDTA solution. Thereafter, cells were centrifuged (2000 × *g*, 5 min) and resuspended in paraformaldehyde in PBS (0.8%, m/v). The mean fluorescence of a total of 10,000 cells was determined with a Beckman Coulter CytoFLEX cytometer (Beckman Coulter, Krefeld, Germany, excitation 488 nm, emission 525–540 nm; FITC channel). The mean fluorescence values of the cells incubated with NPs were standardized by forming a ratio with mean fluorescence values of corresponding control cells. For serum free experiments, culture medium was exchanged to serum free medium 24 h prior to NP incubation.

#### 2.7.3. Determination of cellular interaction after protein adsorption by flow cytometry

In order to analyze the influence of the protein corona of antibody-modified NPs on cellular interaction, NPs were incubated with HS previous to cell exposition. Briefly, $1 \times 10^5$ SK-BR-3 or MCF-7 cells/well were seeded on a 24 well plate and cultivated for 24 h. Cell culture medium was replaced with serum free medium and cells were maintained for another 24 h before NP incubation.

An aliquot corresponding to 0.008 $m^2$ of NPs was diluted to 173 µL with purified water and incubated with 27 µL of HS (70.8 mg/mL) for 30 min at 37 °C under constant shaking (1200 rpm). Immediately after serum incubation, NPs were diluted with serum free cell culture medium to a concentration of 100 µg/mL. Half of the culture medium of two wells was exchanged with each diluted NP suspension, resulting in a final NP concentration of 50 µg/mL per well. The cells were incubated for 4 h and afterwards flow cytometric sample preparation as well as analysis was performed as described above.

#### 2.7.4. Determination of cellular interaction after trastuzumab preincubation by flow cytometry

For verification of receptor-mediated cell interaction of trastuzumab-modified NPs with overexpressed HER2 on SK-BR-3 cells, receptors were blocked with trastuzumab prior to NP incubation. SK-BR-3 cells were seeded and cultivated as described above. In order to block HER2 on the cell surface, cells were incubated with 10 µg/mL of trastuzumab for 1 h. After 1 h, half of the culture medium was replaced with a dilution containing trastuzumab and NPs, resulting in a trastuzumab concentration of 10 µg/mL and a NP concentration of 50 µg/mL. Cells were incubated for 4 h and analyzed by flow cytometry as described above. For experiments under serum free conditions, culture medium was exchanged to serum free medium 24 h prior to NP incubation.

#### 2.7.5. Visualization of intracellular distribution by fluorescence microscopy

For visualization of NP cell interaction, cells were seeded on Falcon® 8 well chamber slides (Corning Inc., Big Flats, NY, USA) with a density of $1 \times 10^4$ cells/chamber and cultivated for 48 h. Subsequently, cells were incubated with the different NP formulations diluted to a concentration of 50 µg/mL with respective cell culture medium for 6 h. After incubation, cells were washed with PBS containing $Ca^{2+}$ and $Mg^{2+}$ ($PBS^{++}$). For staining of cell membrane, cells were incubated with wheat germ agglutinin AF®350 conjugate (125 µg/mL, Biotium Inc., Hayward, CA, USA) for 10 min and washed once again with $PBS^{++}$. Cells were fixed with paraformaldehyde (4%, m/v) for 15 min, washed with $PBS^{++}$ and covered with Vectashield® mounting medium with 4′,6-diamidino-2-phenylindole (DAPI) (Vector Laboratories, Burlingame, CA, USA) for staining of cell nuclei. For visualization, an IX81 fluorescence microscope (Olympus, Hamburg, Germany) with different filter systems was used (filter 1 for DAPI and AF®350: excitation 360–370 nm, dichroic mirror 400 nm, emission 426–446 nm; filter 2 for NP autofluorescence: excitation 460–500 nm, dichroic mirror 505 nm, emission 510–560 nm). Subsequent analysis was performed with cellSens Dimension 1.17 software (Olympus, Hamburg, Germany). For serum free experiments, cell culture medium was replaced with serum free medium 24 h before NP incubation.

### 2.8. Statistical methods

The data are displayed as average value with standard deviation. Unless stated otherwise, all experiments were performed at least in triplicate. Sigma Plot 12.5 software (Systat Software GmbH, Erkrath, Germany) was used for statistical evaluation. Either One Way ANOVA with Holm-Sidak (adjusted) *post-hoc* tests for comparing different groups or two-tailed Student's *t*-test for comparing two groups was applied. The significance was marked as * for $p \leq 0.05$.

## 3. Results

### 3.1. Characterization of antibody-modified nanoparticles

HSA-NP were prepared by a desolvation technique and subsequently modified with different PEG spacers for ligand coupling. For modification, three linear PEG spacers with varying molecular weight as well as sMBS were used. As an active targeting ligand the monoclonal antibody trastuzumab was covalently attached to the spacer in a second modification step. NP properties were characterized and results are summarized in Table 1. Spherical NPs with hydrodynamic diameters between 200

**Table 1**
Physicochemical characteristics of prepared nanoparticles (mean ± SD, $n \geq 3$; * $p \leq 0.05$).

| Particle system | Hydrodynamic diameter [nm] | PDI | Zeta potential [mV] | Amount of bound PEG [%] | Amount of bound antibody [%] |
|---|---|---|---|---|---|
| HSA-NP | 201.9 ± 8.0 | 0.05 ± 0.03 | −33.6 ± 7.2 | – | – |
| HSA-sMBS-Tra-NP | 216.2 ± 13.7 | 0.05 ± 0.05 | −40.6 ± 16.0 | – | 55.9 ± 4.2 |
| HSA-sMBS-IgG-NP | 207.9 ± 10.7 | 0.05 ± 0.02 | −36.6 ± 2.0 | – | 18.1 ± 6.3 |
| HSA-$PEG_3$-Tra-NP | 215.7 ± 9.2 | 0.06 ± 0.04 | −37.3 ± 6.8 | 8.3 ± 5.1 | 49.9 ± 20.6 |
| HSA-$PEG_5$-Tra-NP | 239.5 ± 18.6* | 0.06 ± 0.03 | −43.3 ± 6.3 | 10.8 ± 8.6 | 79.6 ± 6.9 |
| HSA-$PEG_{10}$-Tra-NP | 245.2 ± 13.1* | 0.07 ± 0.04 | −41.4 ± 4.1 | 13.6 ± 3.4 | 90.9 ± 0.9 |

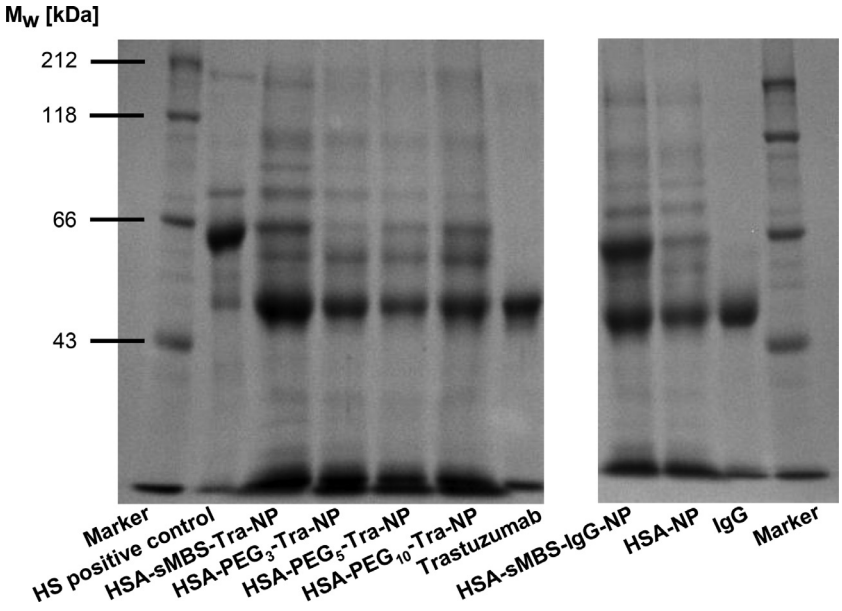


**Fig. 1.** One-dimensional SDS-PAGE analysis of adsorbed human serum (HS) proteins on different HSA nanoparticles.

and 245 nm were obtained (Fig. S4). As an overall tendency, an increasing diameter corresponding with increasing spacer length was observed compared to unmodified HSA-NP. However, only for $PEG_5$- and $PEG_{10}$-modified NPs the hydrodynamic diameter increased significantly ($p \leq 0.05$, Table 1). For all NP formulations the PDI as parameter for particle size distribution was below 0.1 and zeta potentials varied between −30 and −43 mV. The percentages of bound PEG spacer showed no significant differences, although a trend of increasing PEG binding from 8.3 to 13.6% with rising PEG length could be seen (Table 1, Fig. S1). The resulting binding of trastuzumab and IgG as a negative control was analyzed by SEC (Table 1, Fig. S2). As a tendency it was observed that a longer PEG spacer resulted in higher binding of the antibody trastuzumab (50% for $PEG_3$ to 91% for $PEG_{10}$ modification).

### 3.2. Protein adsorption on antibody-modified nanoparticles

#### 3.2.1. SDS-PAGE identification of corona proteins

In order to characterize corona proteins, one-dimensional SDS-PAGE was performed. Native HS as a control, and the desorbed corona proteins of HSA-NP, as well as antibody-modified HSA-NP with different crosslinkers were analyzed. Fig. 1 shows the distinct protein patterns for the tested NPs. For HS control, the most intense band was HSA with a molecular weight of 66.5 kDa. In comparison to that, the HSA bands for NP systems were less intense but other additional bands appeared. Furthermore, all tested NP formulations showed the same band pattern but with different intensities. The most intense signals were detected for HSA-sMBS-Tra-NP and HSA-sMBS-IgG-NP, whereas bands for PEGylated NPs were less intense.

#### 3.2.2. LC-MS/MS identification of corona proteins

Data-dependent LC-MS/MS analysis was used to gather more information on protein identities, their corresponding physiological functions and other characteristics. In total, a number of 246 different proteins were identified in the NP protein coronas (Table S5-S7). The highest number of different proteins was detected on HSA-NP (202) and HSA-sMBS-Tra-NP (201, Fig. 2A). The lowest number was identified on HSA-$PEG_{10}$-Tra-NP (153, Fig. 2A). When comparing PEGylated to unmodified HSA-NP, it could be noted that PEGylation led to less different proteins adsorbed (Fig. 2A). Furthermore, the number of different proteins decreased with increasing PEG spacer length from 167 for $PEG_3$ to 153 for $PEG_{10}$ (Fig. 2A).

A total of 18 proteins were only identified in HS control samples, whereas for NPs only very few totally unique proteins for one corona alone were verified. Regarding the NP coronas, most unique proteins were identified for HSA-NP (8) and only one or none was identified for PEGylated NPs (Fig. 2A).

In Fig. 2B identified corona proteins are depicted according to their physiological function. The percentage distribution of physiological functions was in general similar for all tested NPs. By far the largest number of detected corona proteins is related to initiation of immune response (IR). Generally, NPs enriched IR proteins, as the portion of identified IR proteins increased to 78–81% for NPs compared to 66% in HS control sample. Other physiological functions including lipoproteins and blood coagulation-related proteins were nearly equally distributed at around 5% for each NP system.

Comparing the distribution of the average molecular weight of the detected proteins, the biggest fraction consisted of proteins with an average below 29 kDa (68–74% for NPs and 50% for HS control, Fig. 2C). Compared to HS control, the relative amount of NP corona proteins with an average molecular weight between 29 and 66 kDa (12–16% for NPs and 30% for HS control sample) declined in favor of proteins below 29 kDa.

#### 3.2.3. LC-MS/MS quantitation of corona proteins

Data-independent SWATH LC-MS/MS analysis was employed for quantitation of exemplary proteins. Five proteins covering different

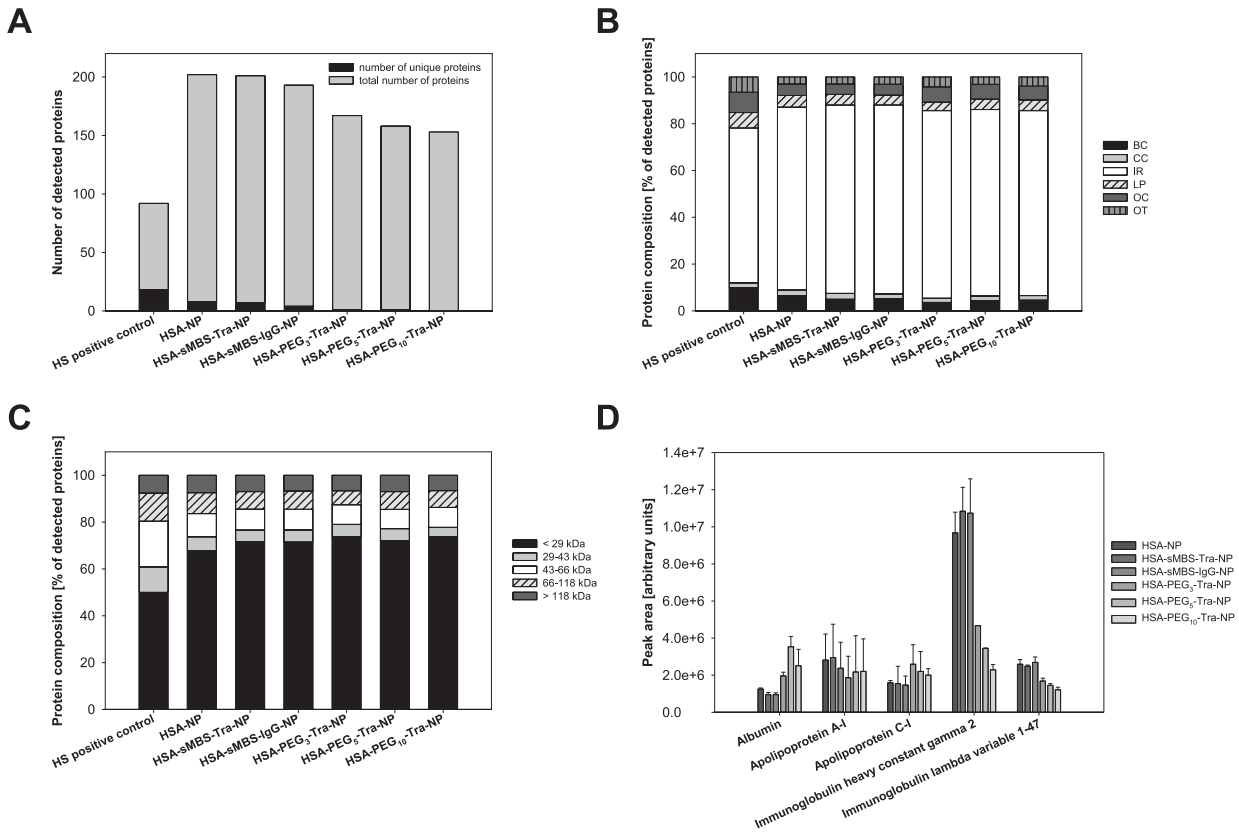


**Fig. 2.** (A) Total number of identified corona proteins with number of unique proteins for respective NP system and classification of the corona proteins according to (B) their physiological function and (C) their average mass. Proteins were identified in two independent experiments by LC-MS/MS in a data-dependent acquisition approach using different NP batches of each formulation for protein corona formation. (D) Quantitation of exemplary corona proteins of the tested NP formulations. For each protein one representative peptide is depicted (Table S4). Proteins were analyzed in two independent experiments by LC-MS/MS in a data-independent acquisition approach (mean ± SD, n = 2). BC = blood coagulation-related proteins, CC = cellular components, IR = immune response initiating proteins, LP = lipoproteins, OT = oxygen transport-related proteins, OC = other components.

physiological functions were selected for quantification according to the peak area of representative peptides. Each of these proteins was also identified in every sample by DDA measurement (Table S5). For every protein, one representative peptide precursor (Table S4), fulfilling the before defined quality criteria, was selected and depicted in Fig. 2D. Extracted Skyline ion chromatograms of the chosen peptides are displayed in Fig. S3. As illustrated in Fig. 2D, PEGylated NPs adsorbed more albumin compared to unmodified HSA-NP and NPs modified with sMBS crosslinker. For quantified lipoproteins, similar amounts of apolipoprotein A-I and apolipoprotein C-I were encountered for all NP systems (Fig. 2D). In contrast to that, the quantity of adsorbed exemplary immunoglobulins was reduced intensively for PEGylated NPs. Compared to HSA-NP, the amount of adsorbed immunoglobulin heavy constant gamma 2 was decreased by 52% for $PEG_3$ modification up to 76% for $PEG_{10}$ modification. The quantity of adsorbed immunoglobulin lambda variable 1–47 was reduced by 35% for $PEG_3$ modification and up to 52% for $PEG_{10}$ modification (Fig. 2D).

### 3.3. Cell culture studies

Two breast cancer cell lines with different HER2 expression (SK-BR-3 and MCF-7) were used for cell interaction studies of antibody-modified NPs. To ensure that NP systems showed no cytotoxic effects, a WST-1 assay was performed. In all experiments a cytotoxicity on the chosen breast cancer cells was not detectable (Fig. S5).

#### 3.3.1. Cellular interaction under varied culture conditions

After incubating SK-BR-3 cells for 24 h with the different NP formulations, $HSA_{PF}$-sMBS-Tra-NP exhibited a higher mean fluorescence under serum free conditions than all other samples (Fig. 3A). As a further tendency, it was observed that shorter linkers led to more pronounced cell interaction for trastuzumab-modified NPs. Hence, $HSA_{PF}$-sMBS-Tra-NP showed the best results followed by the PEGylated NPs according to their spacer lengths. In comparison to that, under serum containing conditions cells incubated with $HSA_{PF}$-$PEG_5$-Tra-NP did display the highest mean fluorescence after 24 h, followed by $HSA_{PF}$-$PEG_3$-Tra-NP (Fig. 3B). MCF-7 cells showed the same tendency as SK-BR-3 cells after incubation with NPs under serum free conditions, but with much lower fluorescence intensities (Fig. 3C). The shorter the PEG chain and linker, the higher was the measured mean fluorescence. It was particularly noticeable that the IgG-modified NP formulation with sMBS as crosslinker showed comparable mean fluorescence rates to trastuzumab modification. After FBS supplementation, mean fluorescence values of MCF-7 cells were comparable to untreated control cells for all NP systems over the time period of 24 h (Fig. 3D).

In addition to flow cytometry, fluorescence microscopy was used to achieve a qualitative impression on intracellular nanoparticle distribution (Fig. S6 + S7). Corresponding to FACS analysis, serum free and serum containing conditions were analyzed. NPs were visualized as green fluorescence signal. Under serum free conditions SK-BR-3 cells incubated with HSA-sMBS-Tra-NP exhibited the most intensive green fluorescence signal (Fig. S6A). No notable difference was detected within NPs modified with PEG and HSA-sMBS-IgG-NP (Fig. S6B-E). In contrast to that, green fluorescence was mainly detected for HSA-$PEG_5$-Tra-NP (Fig. S6I) and HSA-$PEG_3$-Tra-NP (Fig. S6H) followed by HSA-sMBS-Tra-NP (Fig. S6F) under serum containing conditions. SK-BR-3 cells incubated with the other NP formulations showed nearly no green fluorescence (Fig. S6G+*J*). MCF-7 cells showed less cell interaction with NPs

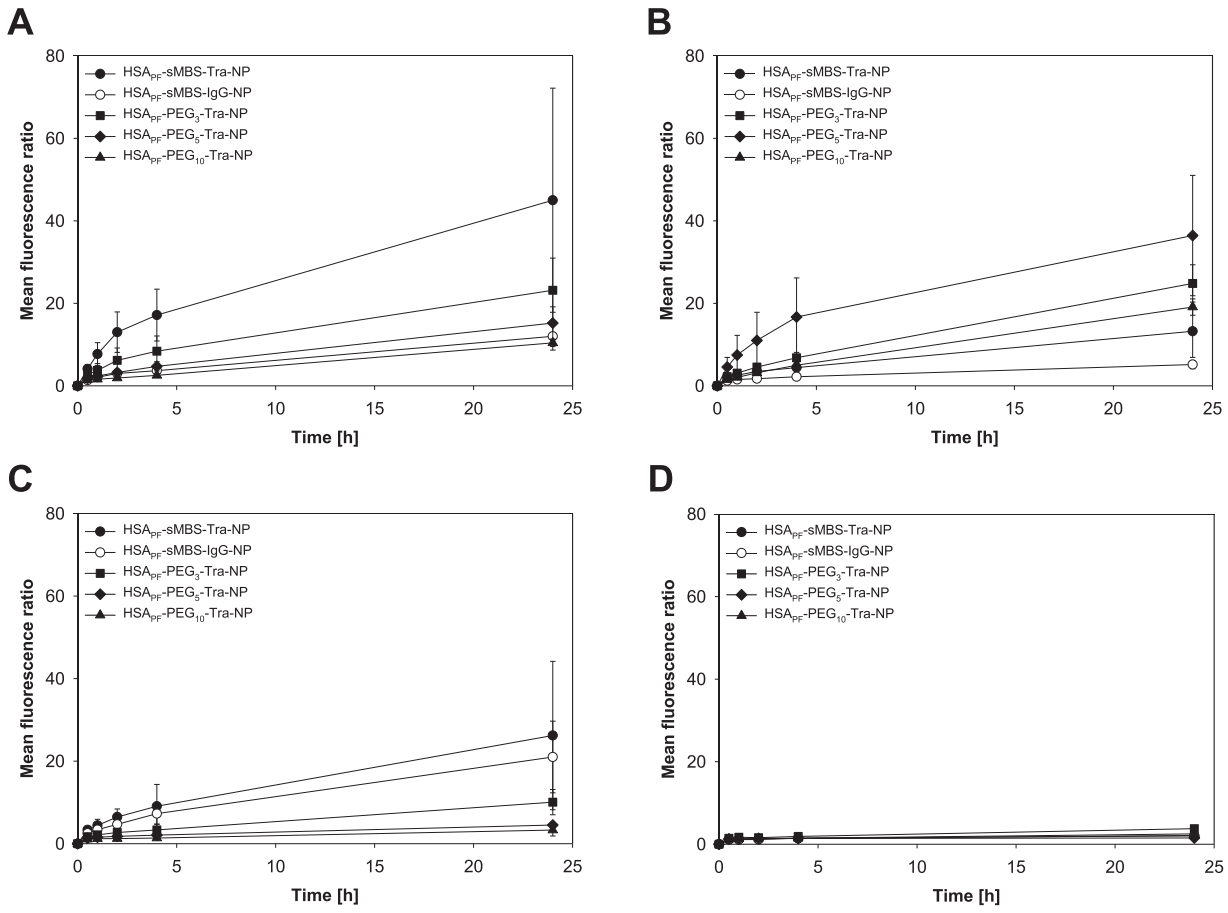


**Fig. 3.** Time-dependent cell interaction of antibody-modified PF-labeled nanoparticles with (*A* + *B*) SK-BR-3 cells and (C + D) MCF-7 cells under (A + C) serum free and (*B* + *D*) serum containing conditions (mean ± SD, n = 3). Results are presented as x-fold increase of the mean fluorescence of untreated control cells.

than SK-BR-3 cells (Fig. S7). Overall, slightly more green fluorescence was detected under serum free conditions (Fig. S7A-E). According to the green fluorescence, the most distinctive cell interaction was achieved with sMBS-modified NPs as already observed with FACS analysis (Fig. S7A + *B*).

### *3.3.2. Cellular interaction after serum preincubation*

The presence of a preformed protein corona was additionally analyzed and compared to the incubation conditions described above (serum free and serum containing, Fig. 4A+B). Looking at the cellular interaction of the different NPs after 4 h under the three different incubation conditions, a significant influence of protein adsorption on SK-BR-3 cell interaction was monitored for HSA$_{PF}$-sMBS-Tra-NP ($p \leq 0.05$, Fig. 4A). For HSA$_{PF}$-PEG$_3$-Tra-NP, no significant effects were detectable, whereas incubation with HSA$_{PF}$-PEG$_5$-Tra-NP and HSA$_{PF}$-PEG$_{10}$-Tra-NP led to an increased cellular interaction under FBS conditions. By comparing NP cell interaction with MCF-7 cells, it was observed that protein adsorption had the strongest influence on sMBS-modified NPs (Fig. 4B). Under serum free conditions mean fluorescence values were considerably higher than for the other incubation conditions. For PEGylated NPs there was hardly any cell interaction detectable after 4 h compared to control cells under all tested conditions.

### *3.3.3. Cellular interaction after trastuzumab preincubation*

Preincubation with free trastuzumab was performed to proof receptor-specific interaction of trastuzumab-modified NPs. As MCF-7 cells do not show relevant HER2 expression, only SK-BR-3 cells were tested. Results show that after trastuzumab preincubation, cell interaction was reduced significantly for all NP systems for both serum free and serum containing conditions ($p \leq 0.05$, Fig. 4C). Additionally, it can be noted that by using sMBS as a crosslinker mean fluorescence values were not as low as for PEGylated NP systems after trastuzumab preincubation.

## 4. Discussion

### *4.1. Characterization of antibody-modified nanoparticles*

HSA-NP were prepared according to a well characterized desolvation technique [26]. HSA as a biodegradable, biocompatible, nontoxic and non-immunogenic endogenous protein is well suited for application as a targeted drug delivery system [27]. Following HSA-NP preparation, NPs were modified with different PEG spacers for ligand coupling. For this purpose, PEG as a FDA approved, water soluble, nontoxic, and biocompatible inactive compound was used [28]. Another advantageous property of PEG is that it prolongs the blood circulation time of nanocarriers due to its stealth effect which was already utilized for the marketed nano-drug Doxil® [13,29]. To evaluate the effect of PEG chain length, three different linear PEG spacers exhibiting the same end groups but different molecular weights, namely 3, 5, and 10 kDa, were used. In addition to PEG, sMBS as shortest possible linker with succinimide and maleimide reactivity for covalent coupling of a targeting ligand and preferably no stealth effect was analyzed. As an active targeting ligand, the monoclonal antibody trastuzumab addressing HER2 was used.

NPs were fully characterized regarding their hydrodynamic diameter, PDI, zeta potential, PEG and antibody binding, as these properties are relevant parameters for NP cell interaction and formation of a protein corona [5,16]. The observed correlation of increasing NP diameter with increasing spacer length compared to native HSA-NP can be

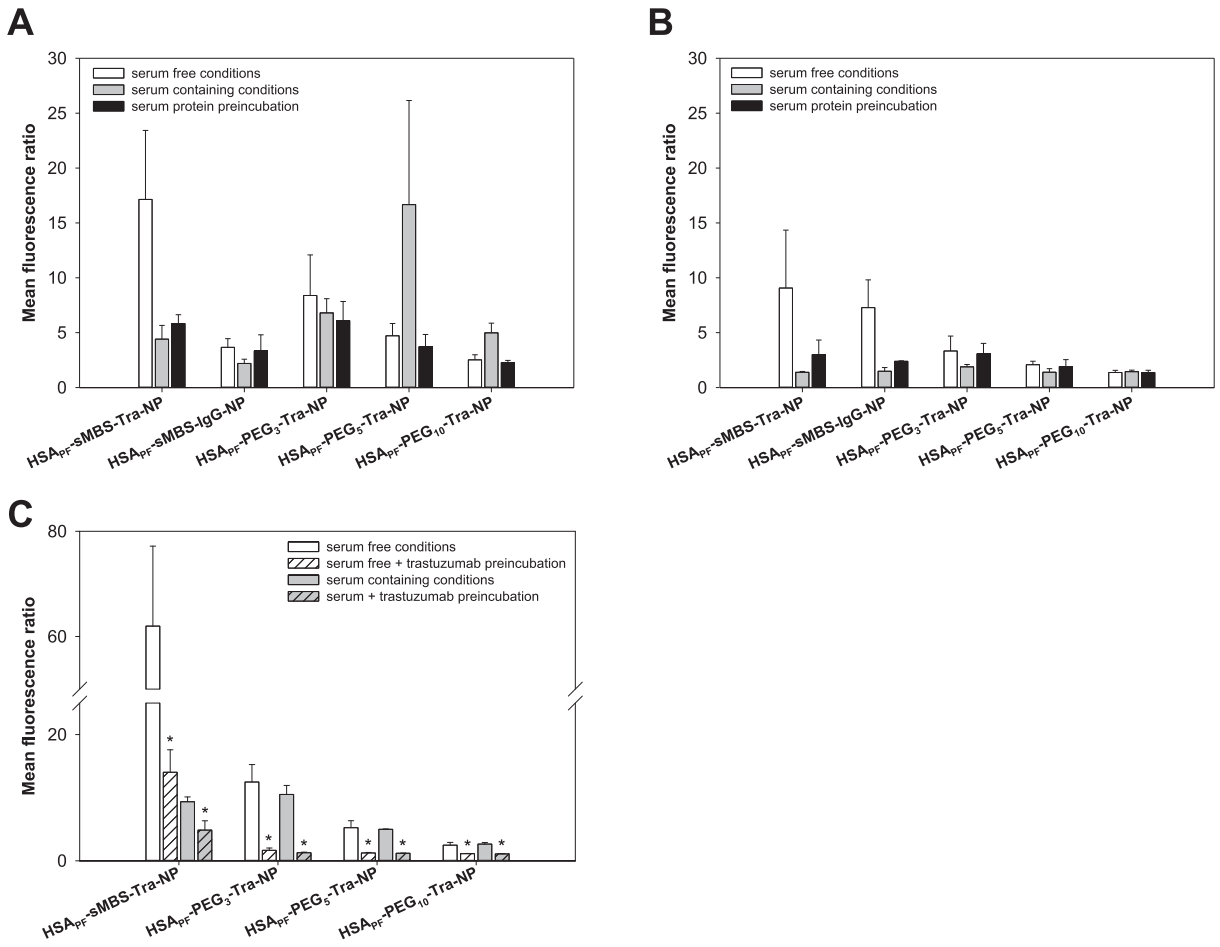


**Fig. 4.** Cellular interaction of antibody-modified PF-labeled nanoparticles after 4 h incubation with (A) SK-BR-3 and (B) MCF-7 cells in different environments: Serum free conditions (white), serum containing conditions (gray), after preincubation with human serum (black; mean ± SD, $n = 3$). (C) SK-BR-3 cell association after 4 h of incubation with trastuzumab-modified PF-labeled nanoparticles with and without trastuzumab preincubation measured by flow cytometry (mean ± SD, $n = 3$; $^{*}$ $p \leq 0.05$). Serum free and serum containing conditions are displayed. All results are presented as x-fold increase of the mean fluorescence of control cells.

explained by the binding of additional water molecules with increasing PEG molecular weight adding to the hydrodynamic diameter [30]. For all NP formulations, a PDI below 0.1 indicated a monodisperse size distribution and with zeta potentials below −30 mV NPs were sufficiently stabilized electrostatically [31].

Three linear PEG crosslinkers with varying molecular weight were analyzed. The aim was on the one hand to find the optimal length for receptor-mediated active targeting on tumor cells. On the other hand, the objective was to obtain minimal effects of serum protein adsorption on the targeting process. For the coupling reaction, the same molar excess of PEG was employed and the percentage of bound PEG was analyzed. The amount of bound PEG was in accordance with previous studies [32]. As only a slight increase of PEG binding with rising PEG length could be observed, the approximately same number of PEG chains was linked per NP independent from PEG length. Hence, the conditions for following antibody binding were comparable. In addition to the linker function for ligands, PEGylation of NPs has several other effects. The grafting density and the molecular weight of the PEG chains also have an effect on serum protein adsorption and on receptor-mediated endocytosis [13,33]. PEGylation also increases colloidal stability through steric repulsion as a function of grafting density and linker length [34,35]. As stated above, in this study the grafting density was nearly constant and only the influence of the molecular weight of the spacer was analyzed.

One disadvantage of PEGylation is a possible hindrance of cellular uptake of nanocarriers [35]. This disadvantage can be alleviated by striving for active targeting with the monoclonal antibody trastuzumab. In addition to trastuzumab modification, an unspecific IgG antibody was used as a control. For specific covalent binding of the antibodies, the maleimide function of the spacer was used. The antibodies were thiolated with Traut's reagent beforehand to guarantee that sufficient sulfhydryl groups are available on the antibody [7]. It was observed that longer spacers resulted in a higher percentage of antibody binding. A possible explanation could be that with increasing linear linker length, the resulting surface increases as well, whereas the curvature of the NPs decreases. These two factors seem to favor the binding of antibodies.

In conclusion, stable antibody-modified NPs were prepared using different crosslinkers for antibody binding.

### 4.2. Protein adsorption on antibody-modified nanoparticles

Although intensive research has been conducted in the last years, the protein corona still remains one of the biggest obstacles in successfully launching nanoparticulate drug formulations on the market [36,37]. Therefore, a closer look on corona proteins could contribute to identify NP parameters which are beneficial for effective active targeting after corona formation. For characterization of corona proteins, one-dimensional SDS-PAGE as well as LC-MS/MS analysis was performed. The corona proteins of HSA-NP, different antibody-modified NPs and the proteins in native human serum were analyzed. As expected, SDS-PAGE analysis revealed that the most intensive band for HS control was

HSA as it is the most abundant protein in HS [38]. In contrast to that, HSA bands for NP systems were less intense. Additionally other bands appeared for the NP samples, showing that NPs could enrich different proteins in their corona compared to the native serum. Most strikingly, all NP systems showed similar band patterns only varying in their intensity. The increased surface hydrophilicity of PEGylated NPs consequently caused less protein adsorption compared to non-PEGylated NPs [39]. In conclusion, these results indicate that the selection of the spacer does not have an influence on the identity of the adsorbed proteins, but mainly affects their quantity.

In addition, data-dependent LC-MS/MS analysis was performed to identify corona proteins and gather more specific information on their corresponding physiological functions and other protein characteristics. This data was used to obtain new insights on favorable NP characteristics and modifications. Many different proteins were identified for all NP samples, but upon PEGylation the number of identified proteins decreased. One example was beta-2-glycoprotein 1, which acts as an opsonin. It was only identified on HSA-NP, but not on PEGylated NPs (Table S5). This was in accordance with a recent publication of our group, where beta-2-glycoprotein 1 was only found in the corona of PLGA-NP, but not in the corona of PLGA-PEG-NP [21]. Moreover, the decrease of identified proteins correlated with PEG spacer length. This finding confirmed the shielding effect of PEG dependent on molecular weight as already noted in many studies [13,33,40]. Nevertheless, many proteins acting as opsonins like immunoglobulins and dysopsonins like apolipoproteins were identified in all NP samples. Pozzi et al. [41] already described that for PEGylated liposomes with different PEG molecular weights most corona proteins were present in all coronas, including non-PEGylated liposomes. These results were confirmed in our present study regarding PEG modification of HSA-NP. In agreement with SDS-PAGE analysis, NP starting material seemed to have the greatest effect on the identity of the corona proteins.

Relating the identified proteins to different physiological functions revealed that by far most proteins of all corona samples were involved in IR. Immune system-related proteins like immunoglobulins and complement factors act as opsonins. They mark NPs for enhanced recognition by the reticuloendothelial system, leading to rapid clearance from blood circulation [18]. One example for initiation of IR is complement C3 protein, which is known as one of the most important components of the opsonin system and was found in all samples (Table S5) [13]. Proteins of other physiological functions were distributed nearly equally. Overall, modification with PEG did only decrease the number of identified proteins but did not affect their relative distribution regarding their physiological functions.

The comparison of the relative molecular weight distribution showed that most proteins had a molecular mass below 29 kDa. These results are in concordance with previous findings for PLGA-NP [21]. NP size and resulting NP curvature are an influencing factor for the identity of corona proteins [15]. According to Mahmoudi et al. [42], proteins with lower molecular weights are attracted to smaller NPs. This is probably because of the higher curvature of small NPs, which creates a greater barrier for larger proteins to adsorb. In contrast to that, our findings demonstrate that NP size did not affect the molecular weight distribution of corona proteins. With slightly increasing NP size, corresponding to a longer crosslinker, a shift towards higher protein molecular weights was not observed.

In summary, qualitative LC-MS/MS analysis demonstrated only slight variations between the differently modified NPs for the adsorbed corona proteins. The identity of the proteins seemed to be rather influenced by the NP matrix HSA and not as much by NP properties like size and surface hydrophobicity, which were varied with modification. PEGylation only led to less different proteins identified.

The total number of detected proteins and the distribution of functions and average molecular weights only display general tendencies of NPs biological identity upon protein adsorption. Information on the actual quantity of each protein and the total amount adsorbed, which are also important for NP destiny, is not provided with the previous data. Therefore, the same NP samples were evaluated with a SWATH LC-MS/MS approach. SWATH enables the possibility to examine retention time-dependent spectra of all possible analytes in a defined $m/z$ range (data-independent acquisition) and correlate them to the data of a spectral library [43,44]. With this correlation, peptides can be identified from the DIA fragment ion maps and quantitation is possible [43]. It has to be stated that peak areas of different peptides are not comparable with each other due to the peptides' individual signal response during LC-MS/MS analysis. The most abundant protein in HS, which also acts as dysopsonin on NPs, is albumin [45]. Favorable effects of high albumin adsorption seem likely as it was already demonstrated that a preformed albumin corona around NPs leads to reduced opsonin adsorption and slower clearance of NPs from the body [35,46]. As albumin adsorption was increased for PEGylated NPs only, PEGylation was superior to sMBS modification with regard to albumin adsorption. Furthermore, two different apolipoproteins, apolipoprotein A-I and apolipoprotein C-I, were analyzed. Apolipoproteins are components of lipoproteins which mediate transport of lipids and cholesterol in the blood and also represent dysopsonins. Hence, they are known to decrease activation of the reticuloendothelial system and phagocytosis [20]. Concerning the quantified apolipoproteins A-I and C-I, the type of crosslinker and modification did not seem to have an influence on adsorption of these dysopsonins. In contrast to that, when quantifying exemplary immunoglobulins, a different tendency was observed. Here, modification with PEG did seem to have a positive effect on the adsorbed protein amount, as it was reduced compared to non-PEGylated NPs. Moreover, a higher PEG molecular weight led to a greater decrease in IR-related proteins as already described by others [30,39]. This confirms that PEGylated NPs still exhibit beneficial stealth effects even if a targeting ligand is attached. On the contrary, sMBS crosslinker was not able to reduce serum protein adsorption and especially adsorption of opsonins and therefore a prolonged blood circulation time cannot be expected.

Overall, the determined relative quantities of the exemplary proteins were in agreement with the identified numbers of different proteins (DDA measurements). The number of proteins related to IR decreased with increasing PEG molecular weight, whereas the total number of lipoproteins nearly remained constant.

### 4.3. Cell culture studies

For cell culture studies two breast cancer cell lines with different HER2 expression levels were used, namely SK-BR-3 cells with overexpression of HER2 [47] and MCF-7 cells with normal HER2 amplification [48]. Cytotoxic effects of the NP formulations were excluded by performing a WST-1 assay.

To analyze the influence of different crosslinkers on cellular interaction, SK-BR-3 cells and MCF-7 cells were incubated with the PF-labeled NP formulations for different periods of time. Thereafter, cells were analyzed by fluorescent activated cell sorting (FACS). Furthermore, fluorescence microscopy images were applied to get a visual impression of NP cell interaction. For both experiments, findings were in good agreement with each other. Two different incubation conditions were examined, namely serum free conditions and serum containing conditions with FBS-supplementation to the culture medium. With supplementation of FBS to the culture medium, proteins form a corona around the NPs. This protein corona can affect or even prevent active targeting completely as described before [5]. Our data indicate that culture conditions could influence specific NP cell interaction, as after supplementation of FBS the extent of cell interaction with SK-BR-3 cells changed for trastuzumab-modified NP formulations. Generally, NPs showed less cell interaction with MCF-7 cells than with SK-BR-3 cells due to the lack of HER2 receptors. However, the formed protein corona after FBS supplementation seemed to inhibit unspecific cell interaction of the NPs with MCF-7 cells completely. In addition, the type of linker and its length are important factors to consider. PEGylation appeared to be superior

to sMBS modification. Upon addition of FBS, cell interaction with SK-BR-3 cells was more intensive for PEGylated NPs depending on PEG molecular weight compared to sMBS modification. Moreover, incubation of MCF-7 cells with HSA-sMBS-Tra-NP and unspecific HSA-sMBS-IgG-NP displayed comparable higher cell interaction under serum free conditions for both NP systems. Hence, unspecific interactions for both sMBS-NP systems were very likely.

From a thermodynamic perspective, there are three major determinants that contribute to the free energy of a system during receptor-mediated endocytosis: first the bending energy of the membrane ($F_{membrane}$), second the specific ligand-receptor interaction ($F_{ligand}$) and third the non-specific energy of the grafted polymer chains ($F_{polymer}$) [49]. During binding of the NPs to HER2, $F_{ligand}$ decreases (specific ligand-receptor interaction), whereas $F_{membrane}$ increases due to deformation processes of the cell membrane. $F_{polymer}$ also increases depending on PEG length. The longer the PEG chain, the more flexible it is and the higher the loss of conformational freedom during receptor binding. For successful endocytosis, the decrease in $F_{ligand}$ must overcompensate the increase of $F_{membrane}$ and $F_{polymer}$ [49]. For longer PEG chains the increase in free energy ($F_{polymer}$) is the limitation for receptor-mediated interaction and can explain why the cellular interaction decreased with PEG chain length under serum free conditions. For HSA-sMBS-Tra-NP the increase in $F_{polymer}$ is lower, thus resulting in higher cellular uptake. Stefanick et al. [50] and Zhao and Feng [9] report the same observations. Shorter PEG linkers facilitate cellular uptake of HER2 targeted nanocarriers in SK-BR-3 cells. The translational and conformational freedom of the ligand is lower with shorter PEG linkers and therefore the entropic penalty is reduced during binding of the nanocarriers to cells. With supplementation of FBS to the culture medium, an additional factor has to be taken into consideration. Cellular interaction of antibody-modified NPs can be affected by the formation of a protein corona [5]. This effect was visible for both tested cell lines and impairment by serum protein adsorption was a lot stronger for sMBS crosslinker. The influence of serum protein adsorption on active targeting processes of NPs is also confirmed in literature [5,18,51].

Because of the observed protein effects, the presence of a preformed protein corona was additionally analyzed and compared to serum free and serum containing conditions. For comparability, the protein corona was matching SDS-PAGE and LC-MS/MS analysis. The protein corona seemed to cover most of the targeting ligands of HSA-sMBS-Tra-NP as active targeting was reduced significantly for SK-BR-3 cells. Interestingly, HSA-$PEG_5$-Tra-NP and HSA-$PEG_{10}$-Tra-NP incubation under FBS conditions led to an increased cellular interaction with SK-BR-3 cells. This effect could be caused by specific proteins in FBS which induce cell interaction, but has to be further investigated. Additionally, it seemed that a lower PEG molecular weight of 5 kDa reduced disturbing protein adsorption but still maintained active SK-BR-3 cell targeting of trastuzumab-modified NPs. Compared to that an intensive receptor-mediated interaction of NPs with MCF-7 cells was generally not expected due to the lack of HER2 overexpression. Therefore, a severe influence of protein adsorption on cellular interaction was not likely, which was demonstrated for PEGylated NPs.

Uptake of NPs with protein corona generally depends on different factors, for example on particle properties, cell type and the environment [37]. SDS-PAGE analysis revealed that most proteins were adsorbed on NPs with sMBS linker. Correspondingly, cell interaction experiments indicated that these NPs were affected the most by formation of a protein corona, as active targeting was severely reduced in SK-BR-3 cells. PEGylation instead shielded protein adsorption successfully and maintained active targeting capabilities. However, if the PEG linker length is chosen too long (10 kDa vs. 5 kDa), cell interaction is generally restricted due to higher entropic penalties upon cell binding [9]. Nevertheless, our evaluation demonstrated that PEGylation with the right molecular weight is superior to sMBS modification.

Preincubation with free trastuzumab was performed to saturate membrane-bound HER2 [7]. Receptors were therefore not available for receptor-mediated endocytosis of trastuzumab-modified NPs. As trastuzumab preincubation reduced cell interaction significantly, specific receptor-mediated active targeting of trastuzumab-modified NPs to overexpressed HER2 was successfully demonstrated independent of the linker and its length. The same findings were described for trastuzumab-modified gold NPs and also for other targeting ligand-receptor combinations like cRGD peptide-modified PEGylated gold NPs [5,52].

Additionally, our results indicated that sMBS modification generally led to increased unspecific cell interaction, as the mean fluorescence remained higher after HER2 blocking compared to PEGylated NPs. This was in accordance with the increased cellular interaction of HSA-sMBS-Tra-NP and HSA-sMBS-IgG-NP with MCF-7 cells. This circumstance can as well be explained with the thermodynamical considerations for NP cell interaction described above. In contrast to modification with sMBS, PEGylation induces a steric and thermodynamic barrier for NP attachment to the cell membrane and $F_{polymer}$ increases upon receptor binding [49]. Another compensating factor decreasing the overall free energy is necessary. The diminution of free energy through specific receptor-ligand binding can compensate this effect [49]. Summarizing these results, a specific interaction through active targeting is more likely for PEGylated NPs than unspecific interaction. For sMBS modification the barrier that needs to be compensated is very low and unspecific cellular interaction becomes more likely. Still, specific active targeting was achieved with all NP formulations.

## 5. Conclusion

In this study we demonstrated that several parameters need to be considered for successful active HER2 targeting of trastuzumab-modified NPs. Different trastuzumab-modified HSA-NP formulations were established by using different linkers, namely sMBS and PEG (3, 5, 10 kDa). We showed that the type of linker for the targeting ligand and its length play a crucial role in the extent of active targeting. Shorter linkers like sMBS seemed favorable, but also led to more unspecific cell interaction. PEGylation instead induced specific cell interaction, but with higher molecular weights less cell interaction was generally achieved.

A second important factor is considering the impact of serum protein adsorption. PEG compared to sMBS minimized protein adsorption, but did not completely prevent it. The chosen PEG linker length had only minimal influence on the identity of the corona proteins, but rather influenced protein quantity. Furthermore, protein adsorption could decrease specific and unspecific cell interaction of HSA-sMBS-Tra-NP. Receptor-mediated cell interaction of PEGylated NPs was affected less.

In summary, by choosing PEG as a linker for an active targeting ligand, it has the advantage of stealth properties. Because of that protein adsorption can be reduced and active targeting can be maintained. For selection of the right PEG molecular weight, the relationship between possible extent of cell interaction and reduced protein adsorption has to be considered. Moreover, other parameters which are possibly affecting protein adsorption and effective active targeting have to be investigated in the future.

## Supplementary materials

Supplementary material associated with this article can be found, in the online version, at doi:10.1016/j.bbiosy.2021.100032.

## References

[1] Schirrmacher V. From chemotherapy to biological therapy: a review of novel concepts to reduce the side effects of systemic cancer treatment (Review). Int J Oncol 2019;54(2):407–19.
[2] Bazak R, Houri M, El Achy S, Kamel S, Refaat T. Cancer active targeting by nanoparticles: a comprehensive review of literature. J Cancer Res Clin Oncol 2015;141(5):769–84.
[3] Souto EB, Doktorovova S, Campos JR, Martins-Lopes P, Silva AM. Surface-tailored anti-HER2/neu-solid lipid nanoparticles for site-specific targeting MCF-7 and BT-474 breast cancer cells. Eur J Pharm Sci 2019;128:27–35.

[4] Bertrand N, Wu J, Xu X, Kamaly N, Farokhzad OC. Cancer nanotechnology: the impact of passive and active targeting in the era of modern cancer biology. Adv Drug Deliv Rev 2014;66:2–25.

[5] Su G, Jiang H, Xu B, Yu Y, Chen X. Effects of protein corona on active and passive targeting of cyclic RGD peptide-functionalized PEGylation nanoparticles. Mol Pharm 2018;15(11):5019–30.

[6] Jassem S, Wang W, Sweet H, Manoukian R, Chow V, Kanakaraj P, Hutterer KM, Kuhns S, Foltz IN, Chen Q, Ferbas J, McBride HJ. Functional and nonclinical similarity of ABP 980, a biosimilar of trastuzumab. Pharm Res 2019;36(12):177.

[7] Steinhauser I, Spänkuch B, Strebhardt K, Langer K. Trastuzumab-modified nanoparticles: optimisation of preparation and uptake in cancer cells. Biomaterials 2006;27(28):4975–83.

[8] Colombo M, Fiandra L, Alessio G, Mazzucchelli S, Nebuloni M, De Palma C, Kantner K, Pelaz B, Rotem R, Corsi F, Parak WJ, Prosperi D. Tumour homing and therapeutic effect of colloidal nanoparticles depend on the number of attached antibodies. Nat Commun 2016;7:13818.

[9] Zhao J, Feng SS. Effects of PEG tethering chain length of vitamin E TPGS with a Herceptin-functionalized nanoparticle formulation for targeted delivery of anticancer drugs. Biomaterials 2014;35(10):3340–7.

[10] Anhorn MG, Wagner S, Kreuter J, Langer K, von Briesen H. Specific targeting of HER2 overexpressing breast cancer cells with doxorubicin-loaded trastuzumab-modified human serum albumin nanoparticles. Bioconjug Chem 2008;19(12):2321–31.

[11] Desai N, Trieu V, Yao Z, Louie L, Ci S, Yang A, Tao C, De T, Beals B, Dykes D, Noker P, Yao R, Labao E, Hawkins M, Soon-Shiong P. Increased antitumor activity, intratumor paclitaxel concentrations, and endothelial cell transport of cremophor-free, albumin-bound paclitaxel, ABI-007, compared with cremophor-based paclitaxel. Clin Cancer Res 2006;12(4):1317–24.

[12] Immordino ML, Dosio F, Cattel L. Stealth liposomes: review of the basic science, rationale, and clinical applications, existing and potential. Int J Nanomed 2006;1(3):297–315.

[13] Gref R, Lück M, Quellec P, Marchand M, Dellacherie E, Harnisch S, Blunk T, Müller RH. Stealth' corona-core nanoparticles surface modified by polyethylene glycol (PEG): influences of the corona (PEG chain length and surface density) and of the core composition on phagocytic uptake and plasma protein adsorption. Colloids Surf B Biointerfaces 2000;18(3–4):301–13.

[14] Lazarovits J, Chen YY, Sykes EA, Chan WC. Nanoparticle-blood interactions: the implications on solid tumour targeting. Chem Commun (Camb) 2015;51(14):2756–67.

[15] Walkey CD, Olsen JB, Guo H, Emili A, Chan WCW. Nanoparticle size and surface chemistry determine serum protein adsorption and macrophage uptake. J Am Chem Soc 2012;134(4):2139–47.

[16] Nguyen VH, Lee BJ. Protein corona: a new approach for nanomedicine design. Int J Nanomed. 2017;12:3137–51.

[17] Partikel K, Korte R, Mulac D, Humpf HU, Langer K. Serum type and concentration both affect the protein-corona composition of PLGA nanoparticles. Beilstein J Nanotechnol 2019;10:1002–15.

[18] Xiao W, Xiong J, Zhang S, Xiong Y, Zhang H, Gao H. Influence of ligands property and particle size of gold nanoparticles on the protein adsorption and corresponding targeting ability. Int J Pharm 2018;538(1–2):105–11.

[19] Keuth J, Nitschke Y, Mulac D, Riehemann K, Rutsch F, Langer K. Reversion of arterial calcification by elastin-targeted DTPA-HSA nanoparticles. Eur J Pharm Biopharm 2020;150:108–19.

[20] Gossmann R, Fahrländer E, Hummel M, Mulac D, Brockmeyer J, Langer K. Comparative examination of adsorption of serum proteins on HSA- and PLGA-based nanoparticles using SDS-PAGE and LC-MS. Eur J Pharm Biopharm 2015;93:80–7.

[21] Partikel K, Korte R, Stein NC, Mulac D, Herrmann FC, Humpf HU, Langer K. Effect of nanoparticle size and PEGylation on the protein corona of PLGA nanoparticles. Eur J Pharm Biopharm 2019;141:70–80.

[22] Weber C, Reiss S, Langer K. Preparation of surface modified protein nanoparticles by introduction of sulfhydryl groups. Int J Pharm 2000;211(1–2):67–78.

[23] Wisniewski JR, Zougman A, Nagaraj N, Mann M. Universal sample preparation method for proteome analysis. Nat Methods 2009;6(5):359–62.

[24] Ludwig C, Gillet L, Rosenberger G, Amon S, Collins BC, Aebersold R. Data-independent acquisition-based SWATH-MS for quantitative proteomics: a tutorial. Mol Syst Biol 2018;14(8):e8126.

[25] Zhang J, Xin L, Shan B, Chen W, Xie M, Yuen D, Zhang W, Zhang Z, Lajoie GA, Ma B. PEAKS DB: de novo sequencing assisted database search for sensitive and accurate peptide identification. Mol Cell Proteomics 2012;11(4):M111010587.

[26] Langer K, Balthasar S, Vogel V, Dinauer N, von Briesen H, Schubert D. Optimization of the preparation process for human serum albumin (HSA) nanoparticles. Int J Pharm 2003;257(1–2):169–80.

[27] Varanko A, Saha S, Chilkoti A. Recent trends in protein and peptide-based biomaterials for advanced drug delivery. Adv Drug Deliv Rev 2020;156:133–87.

[28] Cheng TL, Chuang KH, Chen BM, Roffler SR. Analytical measurement of PEGylated molecules. Bioconjug Chem 2012;23(5):881–99.

[29] Zhang L, Gu FX, Chan JM, Wang AZ, Langer RS, Farokhzad OC. Nanoparticles in medicine: therapeutic applications and developments. Clin Pharmacol Ther 2008;83(5):761–9.

[30] Caliceti P, Veronese FM. Pharmacokinetic and biodistribution properties of poly(ethylene glycol)-protein conjugates. Adv Drug Deliv Rev 2003;55(10):1261–77.

[31] Müller RH, Jacobs C, Kayser O. Nanosuspensions as particulate drug formulations in therapy. Rationale for development and what we can expect for the future. Adv Drug Deliv Rev 2001;47(1):3–19.

[32] Fahrländer E, Schelhaas S, Jacobs AH, Langer K. PEGylated human serum albumin (HSA) nanoparticles: preparation, characterization and quantification of the PEGylation extent. Nanotechnology 2015;26(14):145103.

[33] Pelaz B, del Pino P, Maffre P, Hartmann R, Gallego M, Rivera-Fernández S, de la Fuente JM, Nienhaus GU, Parak WJ. Surface functionalization of nanoparticles with polyethylene glycol: effects on protein adsorption and cellular uptake. ACS Nano 2015;9(7):6996–7008.

[34] Abstiens K, Gregoritza M, Goepferich AM. Ligand density and linker length are critical factors for multivalent nanoparticle-receptor interactions. ACS Appl Mater Interfaces 2019;11(1):1311–20.

[35] Li Z, Wang Y, Zhu J, Zhang Y, Zhang W, Zhou M, Luo C, Li Z, Cai B, Gui S, He Z, Sun J. Emerging well-tailored nanoparticulate delivery system based on in situ regulation of the protein corona. J Control Release 2020;320:1–18.

[36] Francia V, Montizaan D, Salvati A. Interactions at the cell membrane and pathways of internalization of nano-sized materials for nanomedicine. Beilstein J Nanotechnol 2020;11:338–53.

[37] Chen D, Ganesh S, Wang W, Amiji M. Plasma protein adsorption and biological identity of systemically administered nanoparticles. Nanomedicine (Lond.) 2017;12(17):2113–35.

[38] Kratz F. Albumin as a drug carrier: design of prodrugs, drug conjugates and nanoparticles. J Control Release 2008;132(3):171–83.

[39] Knop K, Hoogenboom R, Fischer D, Schubert US. Poly(ethylene glycol) in drug delivery: pros and cons as well as potential alternatives. Angew Chem Int Ed Engl 2010;49(36):6288–308.

[40] Vonarbourg A, Passirani C, Saulnier P, Benoit JP. Parameters influencing the stealthiness of colloidal drug delivery systems. Biomaterials 2006;27(24):4356–73.

[41] Pozzi D, Colapicchioni V, Caracciolo G, Piovesana S, Capriotti AL, Palchetti S, De Grossi S, Riccioli A, Amenitsch H, Laganà A. Effect of polyethyleneglycol (PEG) chain length on the bio-nano-interactions between PEGylated lipid nanoparticles and biological fluids: from nanostructure to uptake in cancer cells. Nanoscale 2014;6(5):2782–92.

[42] Mahmoudi M, Sheibani S, Milani AS, Rezaee F, Gauberti M, Dinarvand R, Vali H. Crucial role of the protein corona for the specific targeting of nanoparticles. Nanomedicine (Lond.) 2015;10(2):215–26.

[43] Gillet LC, Navarro P, Tate S, Röst H, Selevsek N, Reiter L, Bonner R, Aebersold R. Targeted data extraction of the MS/MS spectra generated by data-independent acquisition: a new concept for consistent and accurate proteome analysis. Mol Cell Proteom 2012;11(6):O111016717.

[44] Egertson JD, MacLean B, Johnson R, Xuan Y, MacCoss MJ. Multiplexed peptide analysis using data-independent acquisition and Skyline. Nat Protoc 2015;10(6):887–903.

[45] Bros M, Nuhn L, Simon J, Moll L, Mailänder V, Landfester K, Grabbe S. The protein corona as a confounding variable of nanoparticle-mediated targeted vaccine delivery. Front Immunol 2018;9:1760.

[46] Mirshafiee V, Kim R, Park S, Mahmoudi M, Kraft ML. Impact of protein pre-coating on the protein corona composition and nanoparticle cellular uptake. Biomaterials 2016;75:295–304.

[47] Subik K, Lee JF, Baxter L, Strzepek T, Costello D, Crowley P, Xing L, Hung MC, Bonfiglio T, Hicks DG, Tang P. The expression patterns of ER, PR, HER2, CK5/6, EGFR, Ki-67 and AR by immunohistochemical analysis in breast cancer cell lines. Breast Cancer (Auckl.) 2010;4:35–41.

[48] Lee AV, Oesterreich S, Davidson NE. MCF-7 cells–changing the course of breast cancer research and care for 45 years. J Natl Cancer Inst 2015;107(7):djv073.

[49] Li Y, Kröger M, Liu WK. Endocytosis of PEGylated nanoparticles accompanied by structural and free energy changes of the grafted polyethylene glycol. Biomaterials 2014;35(30):8467–78.

[50] Stefanick JF, Ashley JD, Kiziltepe T, Bilgicer B. A systematic analysis of peptide linker length and liposomal polyethylene glycol coating on cellular uptake of peptide-targeted liposomes. ACS Nano 2013;7(4):2935–47.

[51] Salvati A, Pitek AS, Monopoli MP, Prapainop K, Bombelli FB, Hristov DR, Kelly PM, Åberg C, Mahon E, Dawson KA. Transferrin-functionalized nanoparticles lose their targeting capabilities when a biomolecule corona adsorbs on the surface. Nat Nanotechnol 2013;8(2):137–43.

[52] Dai Q, Walkey C, Chan WCW. Polyethylene glycol backfilling mitigates the negative impact of the protein corona on nanoparticle cell targeting. Angew Chem Int Ed Engl 2014;53(20):5093–6.